Biointerface Research in Applied Chemistry
Open-Access Journal (ISSN: 2069-5837)

Article
Volume 13, Issue 6, 2023, 506

Study and Enhancement of the Optoelectronic Properties of Fe-doped CdS Films Fabricated by the Spin Coating Technique

https://doi.org/10.33263/BRIAC136.506

Ahmed Rmili [1,*], Lahcen Soussi [1], Taoufik Garmim [2], Ahmed Louardi [3], Chaymae Louardi [4], Abdelhadi El Bachiri [4], Hassane Erguig [1]

[1] Laboratory of Materials Physics and Subatomic, Department of Physics, Faculty of Science, Ibn Tofail University, Kenitra, Morocco
[2] Laboratory of condensed Matter Physics (LPMC), Department of Physic, Faculty of Sciences, Chouaïb Doukkali University, El-Jadida, Morocco
[3] Laboratory of Industrial Techniques, Department of Industrial Engineering, Faculty of Sciences and Techniques, Sidi Mohamed Ben Abdellah University, Fez, Morocco
[4] Bio-Geosciences and Material Engineering Laboratory « LBGIM » Ecole Normale Superieure, Hassan II University, Casablanca, Morocco
* Correspondence: ahmed.rmili@uit.ac.ma (A.R.);

Scopus Author ID 35787656400
Received: 14.10.2022; Accepted: 5.01.2023; Published: 31.01.2023

Abstract: In this work, the sol-gel spin-coated technique deposited CdFeS thin films with (x=0 to 0.07) on glass substrates. The effect of Fe doping on the structural, morphological, optical, and electrical properties of CdS films was examined. The XRD patterns revealed that the addition of Fe does not cause any change in the crystalline phase of CdS and all films were polycrystalline with a hexagonal structure of a preferential orientation along the (002) direction. The SEM images showed that the CdS morphology exhibits a dense surface behavior and the crystallite size increases during the incorporation of Fe. The AFM study demonstrated a homogeneous and continuous aspect of the nanocrystalline grains of CdS with a few amounts of voids depending on the Fe doping concentration. The UV-visible spectra showed that the CdS films present high transparency of around 80%. This value could reach 90% when the incorporation of Fe and the band-gap value range from 2.32eV to 2.44eV, depending on the Fe doping concentration. The electrical study showed a minimum resistivity of 4.6 105 Ω. cm for the CdS samples doped with Fe concentration equal to 3%.

Keywords: Fe-doped CdS; buffer layer; Spin-coated; characterization; Optical and electrical properties.

1. Introduction

The photoconductive response of cadmium sulfide, easy elaboration, and low cost potentially allow this material to be used in several existing fields such as gas detectors [1], laser diode, photoconductors [2, 3], photocatalysts [4, 5], non-linear optoelectronic devices[6], and photovoltaic cells [7-9]. CdS is an n-type semiconductor with a high electrical resistivity of 10^6 Ω.cm for un-doped CdS thin films, which are reduced to about 10^2 Ω.cm by dopant [10]. CdS thin films are also characterized by a direct and large band gap energy of about Eg=2.44 eV [11]. These optoelectric properties of CdS thin films offer a great advantage to be used in solar cell applications, especially as buffer layers.

In solar cell technology, it is necessary to prepare CdS material with good conductivity and high optical transmission, reducing solar cell sheet resistance. In addition, in the CdS structure, the sulfur vacancy and cadmium interstitial sites have formed native defects and are responsible for the electrical conductivities of cadmium sulfide. Therefore, the control of the native defects is to contribute to controlling the conductivity of the CdS. Metals doping CdS thin films play an important role in II-VI semiconductors because it allows the reduction of the electrical resistivity with tailored optical properties for significant solar cell applications. Moreover, it has been known that doping of CdS semiconductors with some metallic elements like Tin (Sn^{2+}) [12], aluminum (Al^{3+}) [13], and copper (Cu^{2+}) [14] improves its optical and physical properties.

Pure and doped CdS films are readily deposited by many different techniques, such as Closed Space Sublimation (CSS) [15], SILAR [16], electrodeposition [17], RF- magnetron sputtering [18], chemical bath deposition (CBD) [19], spray pyrolysis [20] and Sol-Gel spin coating [21, 22], this last method is distinguished by many advantages such as the ability to produce large surfaces with a low cost and its simplicity. The literature contains some works, but their number remains limited concerning the Fe-doped CdS thin films. Besides, and to our modest knowledge, no works about Fe-doped CdS films prepared by spin coating method were reported in the literature. However, the preparation method has an important role since the experimental results differ from one method to another. The spin-coating technique stands out because it offers various advantages, such as low cost, simplicity, and the ability to obtain uniform layers with reproducibility and high adherence [23]. The work aimed to inspect the reaction of the [Fe]/[Cd] ratio on the optical, electrical and structural properties of Fe-doped CdS films elaborated by the sol-gel spin-coating technique. Our laboratory successfully used this method to deposit Ni-doped CdS thin films [24].

2. Materials and Methods

2.1. Preparation of samples.

Cadmium sulfide CdS- films doped by the iron at various [Fe]/[Cd] ratios have been fabricated using the sol-gel associated with a spin coating method using the following precursors; cadmium acetate $Cd(CH_3COO)_2$ for cadmium ions source and thiourea $CS(NH_2)_2$ for sulfur ions without modification. Firstly, we dissolved $Cd(CH_3COO)_2$ and $(SC(NH_2)_2)$ in 50 mL of 2-methoxy-ethanol, and after, 2.42 mL of monoéthanolamine (MEA) was added with molar ratios of [MEA]/[Cd] equal 2. Secondly, it was stirred magnetically at room temperature for 20 minutes to have a homogeneous clear yellow solution. Third, the obtained solution was divided into four parts to introduce the iron chloride as a source of Fe ions with different molar ratios $[Fe^{2+}]/[Cd^{2+}]$ varied from 0%, 1%, 3%, 5%, and 7%. Finally, we put the solution on a well-cleaned glass substrate and spun it at a speed of 3600 rpm for 40 s. The sample was then placed on a hot plate at a temperature of 150°C and dried for 15 minutes. The spin-coating process was repeated six times to reach a fairly thick layer. The film was annealed at 400°C for one hour. Figure 1 describes the experimental procedure used to prepare Fe-doped CdS films.

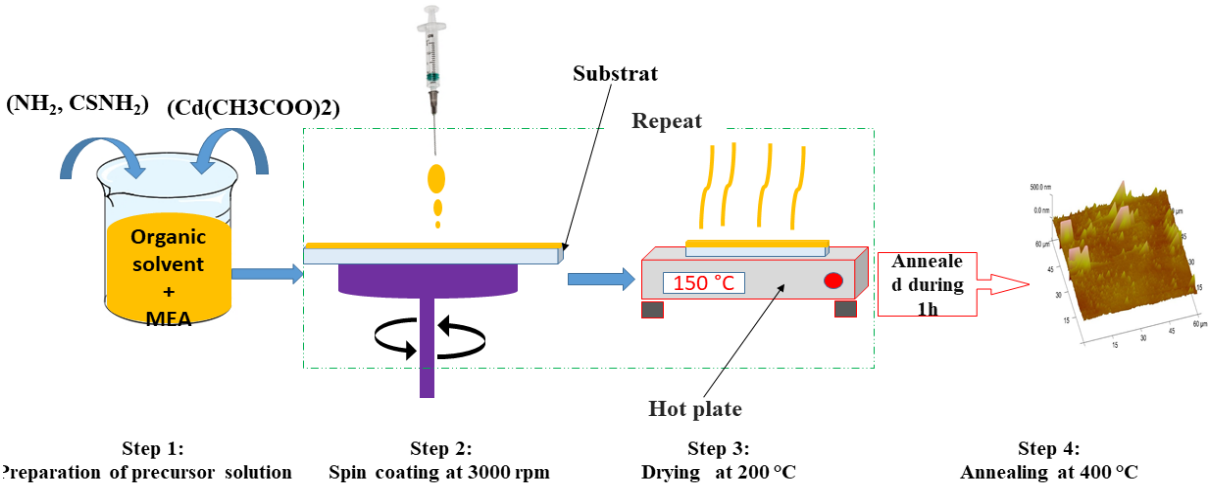

Figure 1. Experiment dispositive to prepare Fe-doped CdS films.

2.2. Characterization.

From the XRD patterns found with CuKα radiation by varying 2θ between 10° and 70°, we deduced the crystal structure of pure and Fe-doped CdS films. The morphology of the samples was described using SEM analysis. Based on the 2D and 3D images recorded by AFM, we visualized the roughness of the Fe-doped CdS film surface. At the same time, the UV-vis spectrophotometer JENWAY6715 was used to determine the optical characterizations with a wavelength ranging from 250 to 1000 nm. The electrical resistivity of samples was measured by the four-point technique.

3. Results and Discussion

3.1. Structural properties.

Figure 2 presents the X-ray diffraction patterns of the Fe-doped CdS thin films doped with different iron concentrations (0, 1, 3, 5, and 7 at.% of Fe). The X-ray diffraction patterns exhibit multiple diffraction peaks, located at 2θ= 24.86°, 26.66°, 28.29°,30.40°,36.62°, 43.91°, 47.78°, and 51.98°, which correspond respectively to the (100), (002), (101), (200), (102), (110), (112) and (103) planes according to the (JCPDS card N°: 77/2306), indicating the polycrystalline structure with [002] as the preferred orientation of pure and doped CdS samples. We noticed that with increasing Fe composition to more than 3at. %, a new peak located at 2θ = 23.73° appears corresponding to the secondary phase of Fe_2O_3. No others peaks corresponding to other phases, such as CdO, were detected.

The iron doping concentration also leads to the variation of the (002) peak intensity; the highest intensity value was found for the samples prepared with the [Fe]/[Cd] ratio equal to 1, indicating a good crystalline quality of the film compared to the other ones. For higher values of [Fe]/[Cd] ratio, the peaks become less intense. This is perhaps due to the degradation of the layer crystallinity. The same results are found by T. Chtouki *et al*. for Ni-doped CdS [24]. On the other hand, Figure 2 shows a slight shift of the diffraction peak (002) towards a higher Bragg angle, confirming the substitution of Cd by Fe ions. This shift clarified in Figure 3 is the result of the creation of a structural strain by the impact of Fe dopant; the strain formula is calculated as follows [25]:

$$\varepsilon_s = -\Delta(\theta_{(002)})\, cotg(\theta_{(002)}) \qquad (1)$$

The latter strain is the outcome of a compressive stress σst which can be determined by:

$$\sigma_{st} = (3\varepsilon_s)B \qquad (2)$$

with B is the bulk modulus of CdS, its value is around 69.44 GPa. Both Figure 4 and Figure 5 display the variation of the strain and the stress of these layers as a function of the iron concentration.

As can be seen, the strain and stress in the films undergo a slight increase for [Fe]/[Cd] ratio between 0 and 3% Fe, which may be that Fe^{2+} ions substitute Cd^{2+} ions. When [Fe]/ [Cd] ratio exceeds 5%, the strain, and the stress decrease, indicating the incorporation of Fe ions in the interstitial crystallographic sites. Figure 4 also manifests that the compressive stress alternates between - 0.10 and 0.35 GPa for doped samples. These stress values create a partial structural change from hexagonal to cubic structure with the appearance of the (200) cubic peak, leading to a slight decrease in the lattice parameters (Table 1).

a and c parameters were determined from the position of the peak based on the formula of the hexagonal system (Eq. 3) and were found to be: a = 4.123 Å and c = 6.707 Å, which are in agreement with the ones reported in the literature [26]:

$$\frac{1}{d_{hkl}^2} = \frac{4(h^2 + k^2 + hk)}{3a^2} + \frac{l^2}{c^2} \qquad (3)$$

The (D_{hkl}) crystallites size of CdS films was calculated from the diffraction patterns of X-ray by the Scherrer equation (Eq. 4) [27]:

$$D_{hkl} = 0.9\frac{\lambda}{\beta_{hkl}\cos(\theta_{hkl})} \qquad (4)$$

where (λ = 1.5406 Å), is the wavelength of X-ray radiation, β_{hkl} is the intrinsic width of half-maximum (FMWH) of the peak, and θ_{hkl} is the angle of diffraction. These calculated results are shown in Table 1.

Table 1 also shows the sizes of the calculated average crystallite of CdS films from the Scherrer formula. As it can be noticed, the average crystallite size increases for [Fe]/[Cd] ratio less than 3 at.% indicating the improvement of CdS crystalline quality. Then, the [Fe]/[Cd] ratio of more than 3at.% decreases due to the degradation of the CdS film crystallinity.

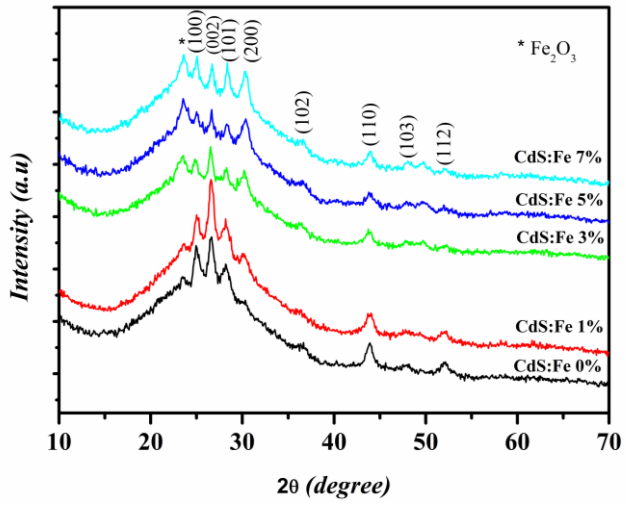

Figure 2. XRD patterns of CdS layers elaborated with various [Fe]/[Cd] ratios (0, 1, 3, 5, 7%).

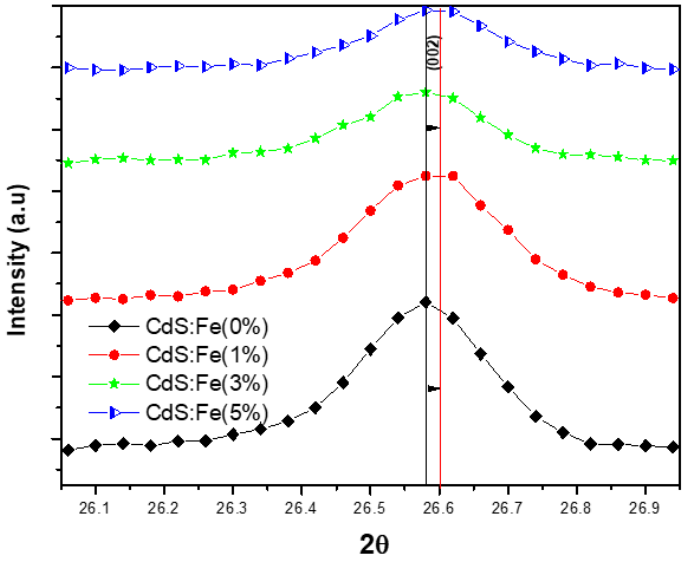

Figure 3. (002) peak position of CdS samples with various [Fe]/[Cd] ratios (0, 1, 3, 5%).

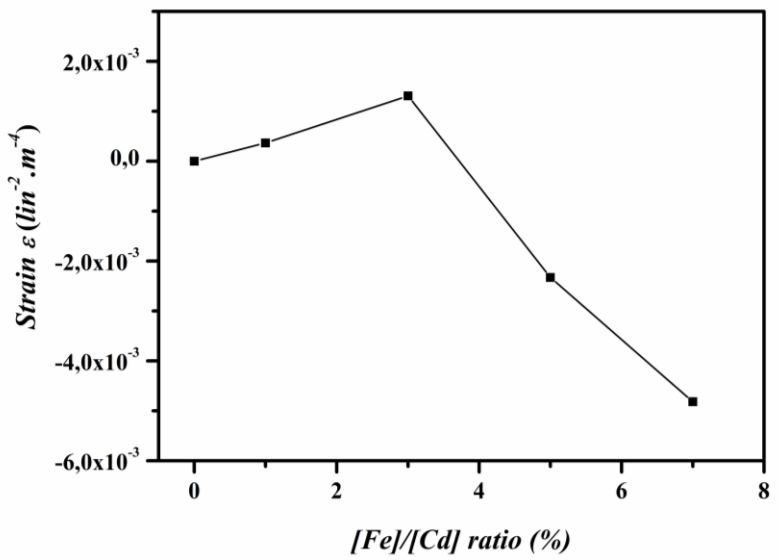

Figure 4. Variation of the structural strain of CdS samples with [Fe]/[Cd] ratios (0, 1, 3, 5, 7%).

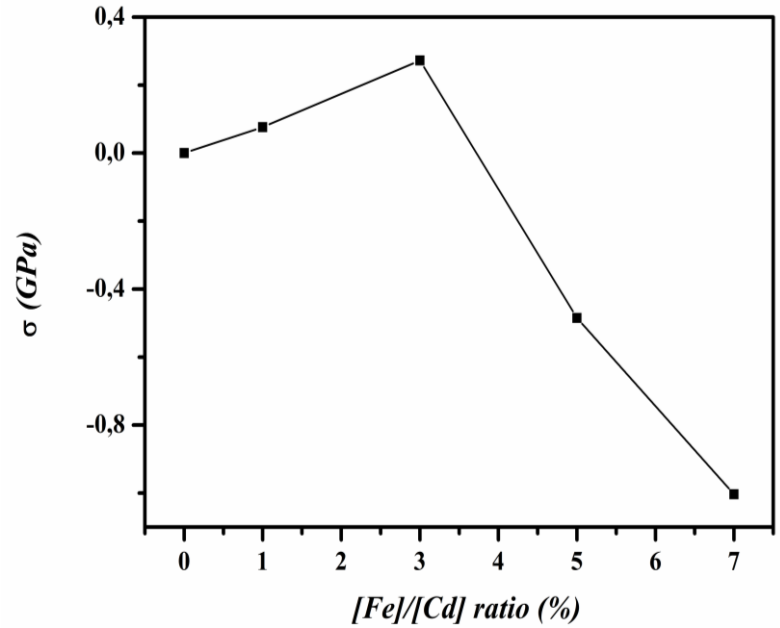

Figure 5. Variation of the structural stress of CdS samples with [Fe]/[Cd] ratios (0, 1, 3, 5, 7%).

Table 1. Lattice parameters and average crystallite sizes of the films with [Fe]/[Cd] ratios (0, 1, 3, 5, 7%).

[Fe]/[Cd] ratio	Experimental	ASTM	Experimental	ASTM	
CdS : 0% Fe	4.123	4.140	6.707	6.715	22.68
CdS : 1% Fe	4.076	4.140	6.710	6.715	27.21
CdS : 3% Fe	4.132	4.140	6.716	6.715	34.01
CdS : 5% Fe	4.102	4.140	6.692	6.715	22.68
CdS : 7% Fe	4.105	4.140	6.675	6.715	17.12

3.2. Morphological properties.

Figure 5a–d shows SEM images of the surface of the Fe-doped CdS layers. It is apparent that all the layers' morphology has relatively smooth surfaces with a few voids and tightly packed grains. The grains' size and surface morphology depended on Fe doping. For the films prepared with 1% and 3% of Fe doping composition, the surface morphology is homogeneous with uniformLy distributed grains indicating the film's good morphological properties quality compared to the others.

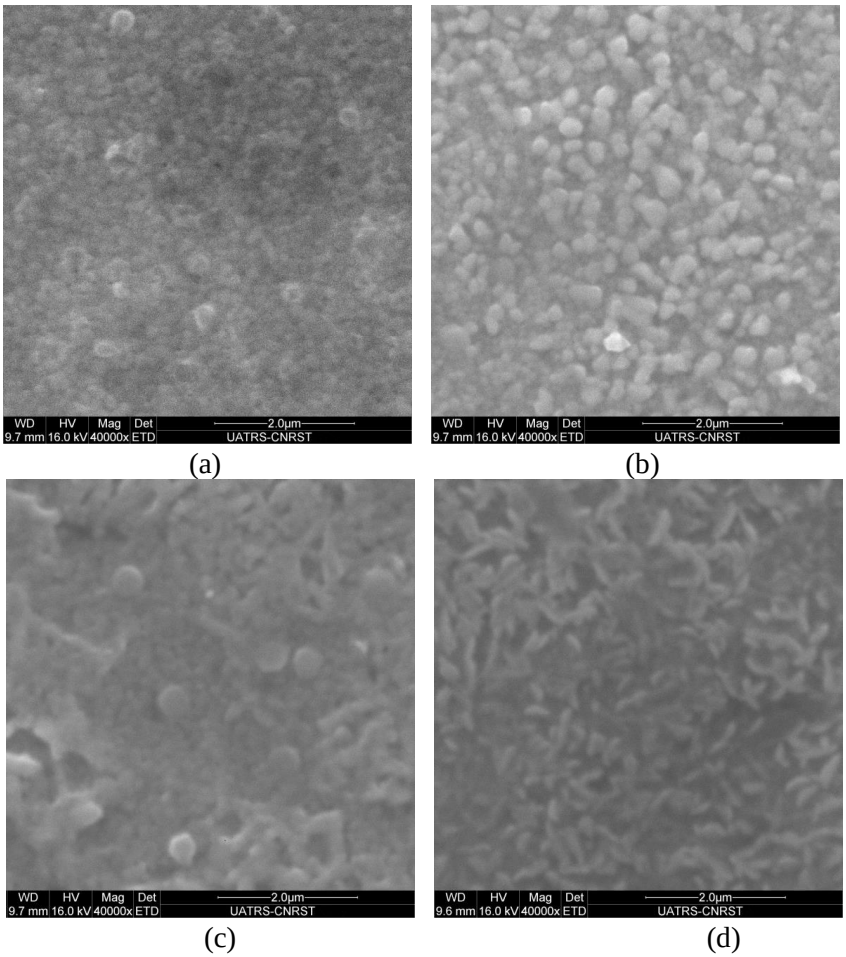

Figure 6. SEM images of CdS:Fe films with [Fe]/ [Cd] ratios: (**a**) CdS, (**b**) 0.01, (**c**) 0,03, and (**d**) 0,05.

The (2 & 3D) dimensional AFM images of the spin-coated Fe-doped CdS films were explored by atomic force microscopy in Soft Tapping Mode. Figure 7 (a and b) shows the (2 & 3D) dimensional AFM micrographs of the Fe-doped CdS layers with [Fe]/[Cd] ratios of 3% and 5%. As can be seen, the Fe-doped CdS samples reveal rather continuous and homogeneous nanocrystalline grains with a few amount of voids. A small number of islands appeared, particularly for the samples deposited with [Fe]/[Cd] ratio of 5%. The roughness value of the root means square (RMS), extracted from AFM data, was evaluated at about 20.84 nm and

40.74 nm for the films elaborated with [Fe]/[Cd] ratio of 3% and 5%, respectively, suggesting that the RMS value is affected by the Fe doping concentration. This change in the surface roughness value may be due to the formation of the Fe_2O_3 secondary phase, as it was detected from the XRD spectra.

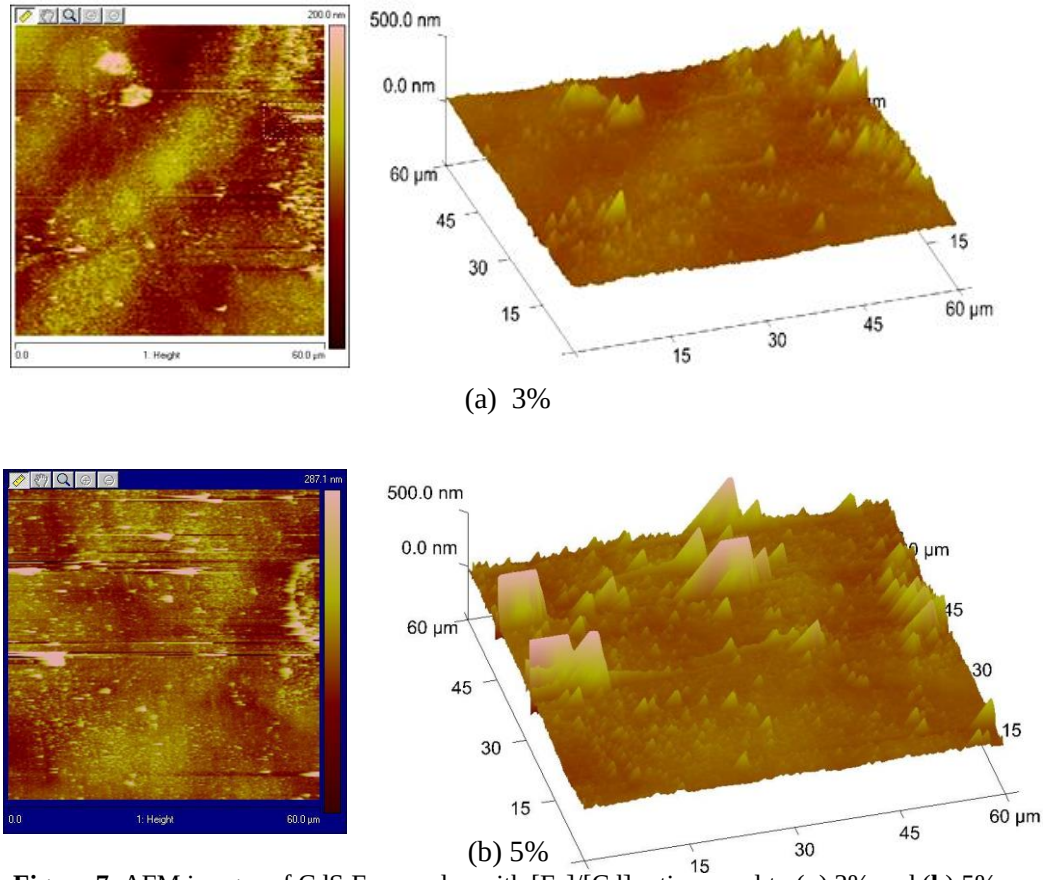

Figure 7. AFM images of CdS:Fe samples with [Fe]/[Cd] ratios equal to (**a**) 3% and (**b**) 5%.

3.3. Compositional analysis.

Figure 8 displays the EDAX spectrum of the doped CdS films with (3% and 5% Fe). The figure displays peaks of Cd, S, Fe, and some impurities like Si, Na, and O, which probably come from the glass substrates and deionized water. The atomic concentration is calculated from the analysis of EDAX and tabulated in Table 2. It was found that the film was non-stochiometric with a slight deficiency of sulfur, due probably to the presence of sulfur vacancies in the prepared films, which plays the role of a donor, giving the n-type conductivity.

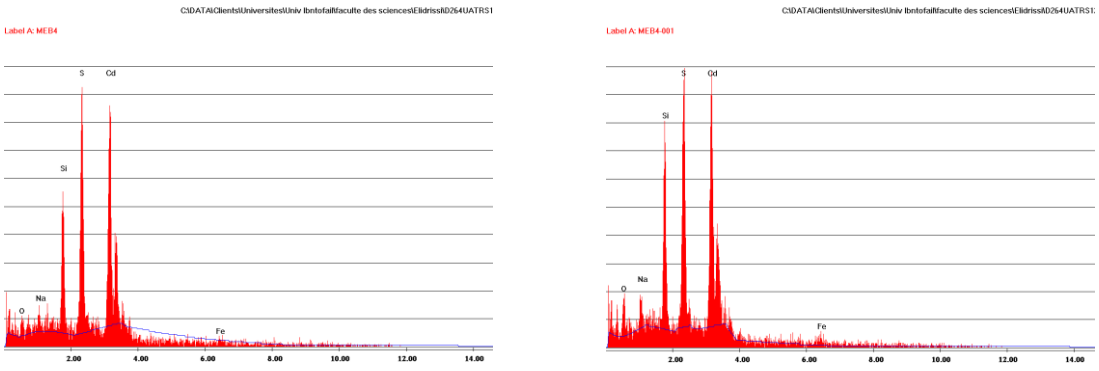

(**a**) (**b**)

Figure 8. EDAX spectrum of sample CdS doped with (**a**) 3% Fe and (**b**) 5% Fe.

Table 2. Atomic concentrations from EDAX analysis and the atomic ratio of the CdS samples with 3% and 5% Fe.

Element		S	Cd	Fe	S/(Cd+Fe)
Atomic percent in the film(at%)	3% Fe	28.42	29.22	2.05	0.91
	5% Fe	28.79	28.90	4.89	0.85

3.4. Optical properties.

An optical study of doped CdS thin layers was done using a UV-VIS spectrometer at room temperature. Figure 9 reveals the optical transmittance curves measured with wavelength varying from 300 to 900 nm using the later equation:

$$T = (1 - R)^2 \exp(-\propto d) \qquad (5)$$

where T is the transmittance, d is the thickness of the film, and R is the reflectance.

The average transmittance of CdS deposited on a glass substrate is found to be in the range of 65–90% for the CdS samples deposited at different [Fe]/[Cd] ratios. However, the optimal optical properties have been obtained for samples with a low doping level; this behavior has been noticed for other semiconductor layers, such as W-doped SnO_2 layers studied by C. Z. Chen *et al*. [28].

High transmittance in the visible range indicates good crystallinity, which makes this material useful as a transparent window layer in CdTe, CIGS, and CZTS-based solar cells, improving photovoltaic efficiency. Similar results were found for Ni-doped CdS material elaborated in our laboratory by spray technique and CdS:Co^{2+} deposited by spin coating studied by K. Veerathangamon *et al*. [29, 30].

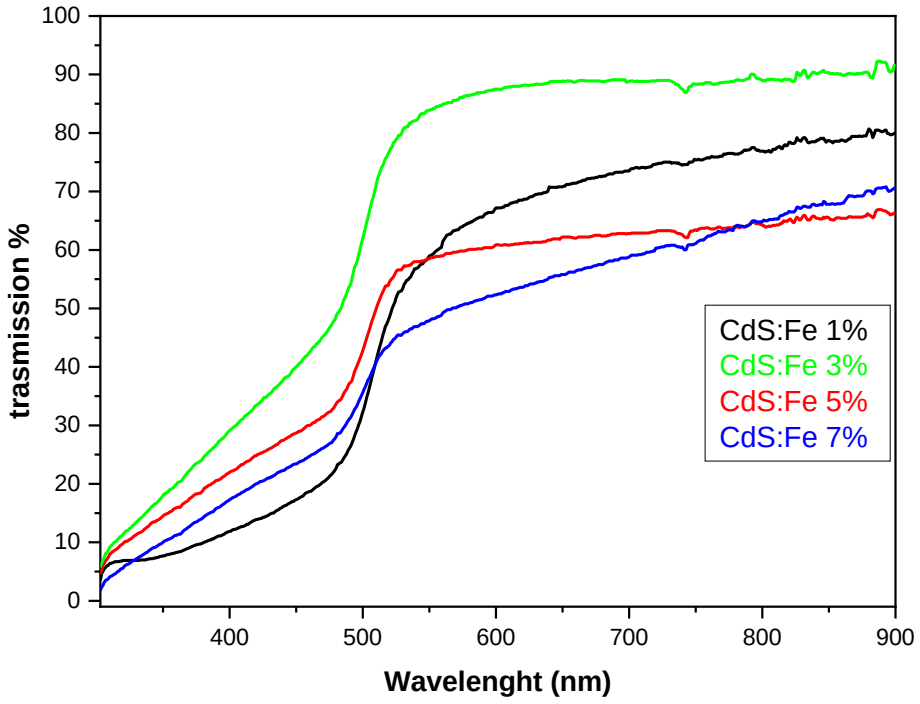

Figure 9. Optical transmittance curves of CdS samples deposited with different Fe concentrations.

The band gap of deposited films is obtained using Tauc's model equation [31]:

$$(\alpha h\nu) = A(h\nu - Eg)^n \qquad (6)$$

where n is equal to ½ for CdS semiconductor, A is a constant, hν is the photon energy, and α is the absorption coefficient.

α is initially calculated by this relation [31]:

$$\alpha = \frac{\ln(T^{-1})}{d} \qquad (7)$$

where d is the thickness of the layer, figure 10 shows the evolution of the absorption coefficient according to wavelength for CdS films synthesized by the spin-coating technic. We can see from this figure that the absorption coefficient decreases with the Fe ratio increase from 1 to 5%. This behavior is mainly due to improvement in the transmittance of CdS films with increasing Fe doping.

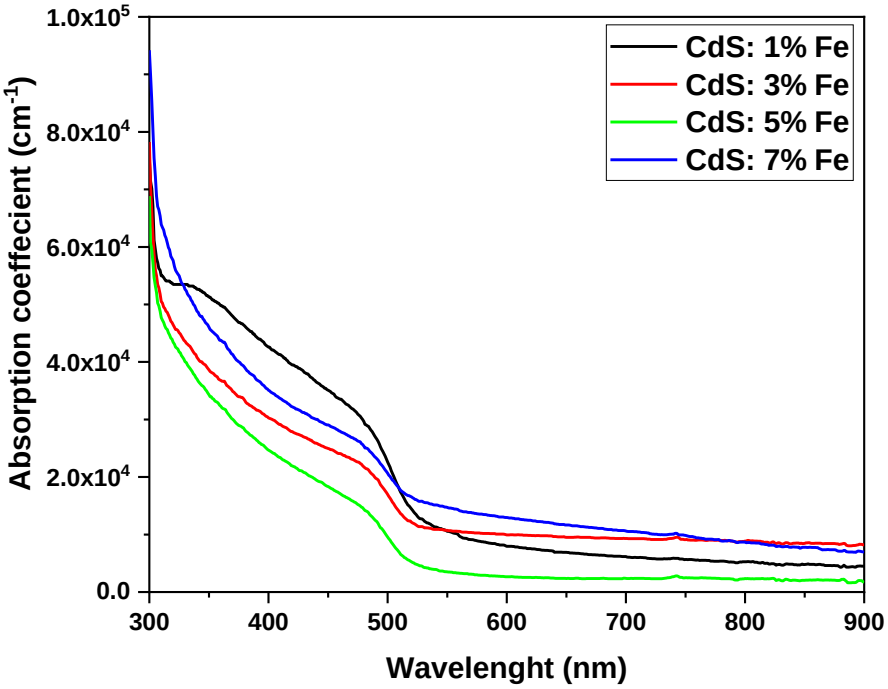

Figure 10. The absorption coefficient of Fe-doped CdS films.

Band gap values E_g were estimated by extrapolating the linear region to $((\alpha h\nu)^2=0)$ of the curves $(\alpha h\nu)^2$ versus $(h\nu)$ presented in Figure 11.

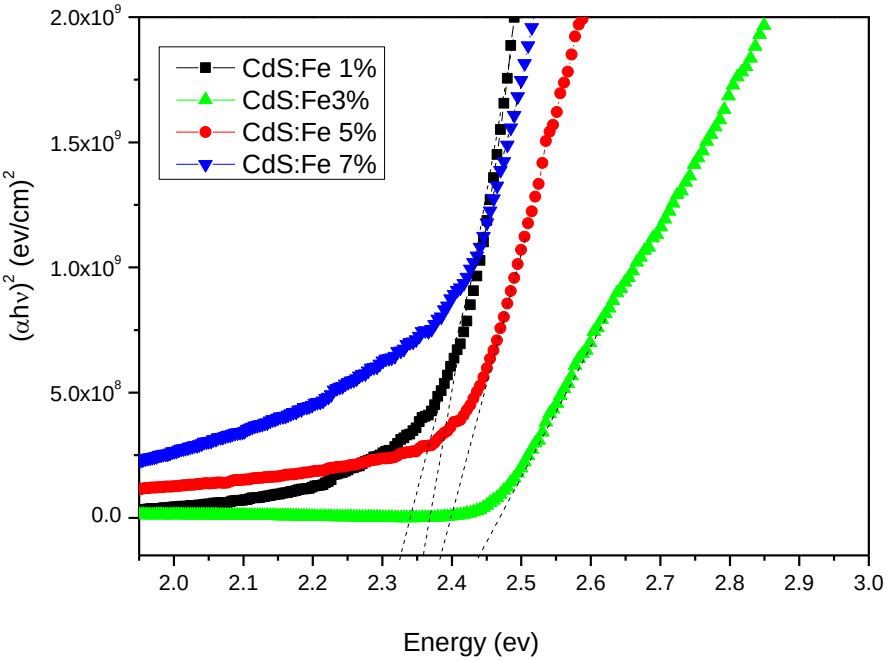

Figure 11. Curves of $(\alpha\ h\ \nu)^2$ versus $h\nu$ of CdS samples with various concentrations of Fe.

Band gap values E_g for the samples deposited with various [Fe]/[Cd] ratios are found to be ranging from 2.32eV to 2.44eV. From the curves, it can be noticed that the band gap initially increases with increasing Fe concentration from 2.37eV for 1% Fe to a maximum of 2.44eV at 3% Fe, which can be explained by the substitution of Cd^{2+} ions by the dopant in the crystalline structure forming a dilute substitution solid solution. Then the value of E_g decrease up to 2.32eV for 7at%. This decrease of Eg may be ascribed to the effect of the ferrite and the exchange interaction between electrons in the sp-d states caused by the effect of magnetic ion Fe^{3+} in the deposited films. S.K.Deshmukh *et al*. found similar results for Fe-doped CdS elaborated by electrodeposition technique [32].

The extinction coefficient of spin-coated Fe-doped CdS thin films was determined from the absorption coefficient and wavelength according to the following relation:

$$k = \frac{\alpha\lambda}{4\pi} \qquad (8)$$

The evolution of the extinction coefficient with respect to wavelength for Fe-doped CdS samples is depicted in Figure 12. This figure shows that k decreases with Fe content increased in CdS. The values of extinction are between 0.02 and 0.2; these values are determined to be similar to those reported in the literature [33, 34].

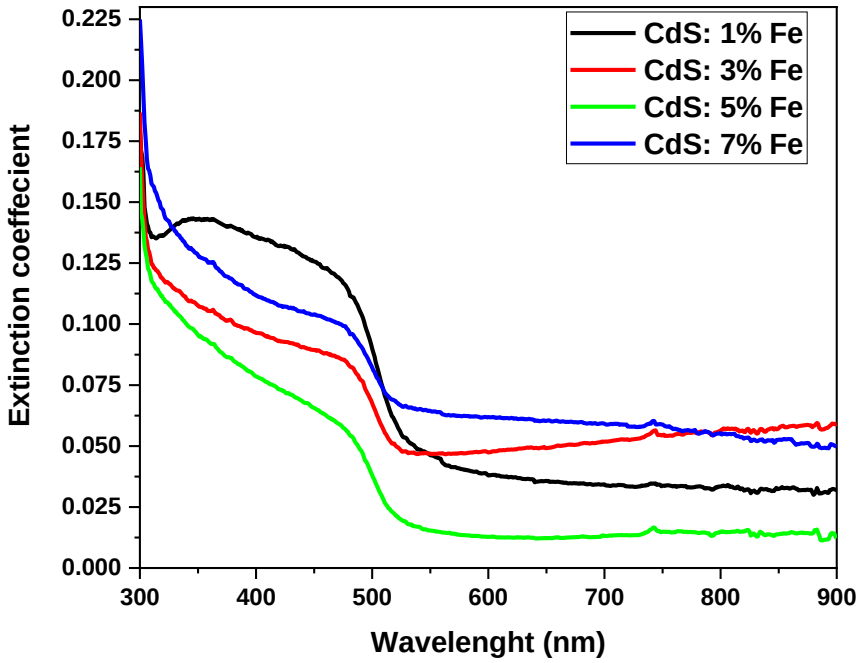

Figure 12. Extinction coefficient of iron-doped CdS films.

Using the reflectance R and k extinction coefficient values, we can calculate the refractive index for obtained doped CdS samples by sol-gel method from this equation [35]:

$$n = \left(\frac{1+R}{1-R}\right) + \sqrt{\frac{4R}{(1-R)^2} - k^2} \qquad (9)$$

Figure 13 illustrates the plot of the refractive index versus wavelength of iron-doped CdS films, such as the Fe ratio varied between 1% and 7%. It can be noticed from this figure that the increase of Fe-doped content in CdS films causes a decrease in refractive index values. The sample doped with 1% represents the highest refractive index, and that doped with 5% has the lowest refractive index. This behavior is similar to absorption coefficient variation.

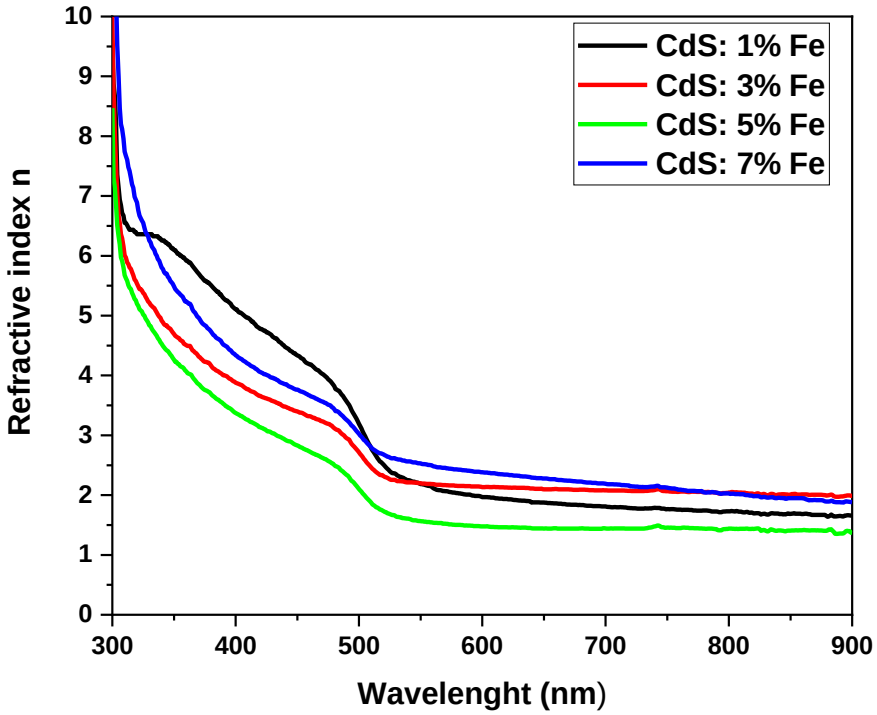

Figure 13. Refractive index of iron-doped CdS films.

The complex dielectric constant is related to optical properties. The real and imaginary part of the dielectric constant of Fe-doped CdS thin films can be calculated from the following relation:

$$\varepsilon = (n^2 - k^2) + (2nk) = \varepsilon_r + i\varepsilon_i \qquad (10)$$

Figures 14 and 15 show the variation of real and imaginary parts for Fe-doped CdS samples to wavelength, respectively. It can be observed from this figure that εr and εi decrease with increasing Fe-doped content in CdS. This indicates the increase of band gap energy according to the incorporation of Fe ions.

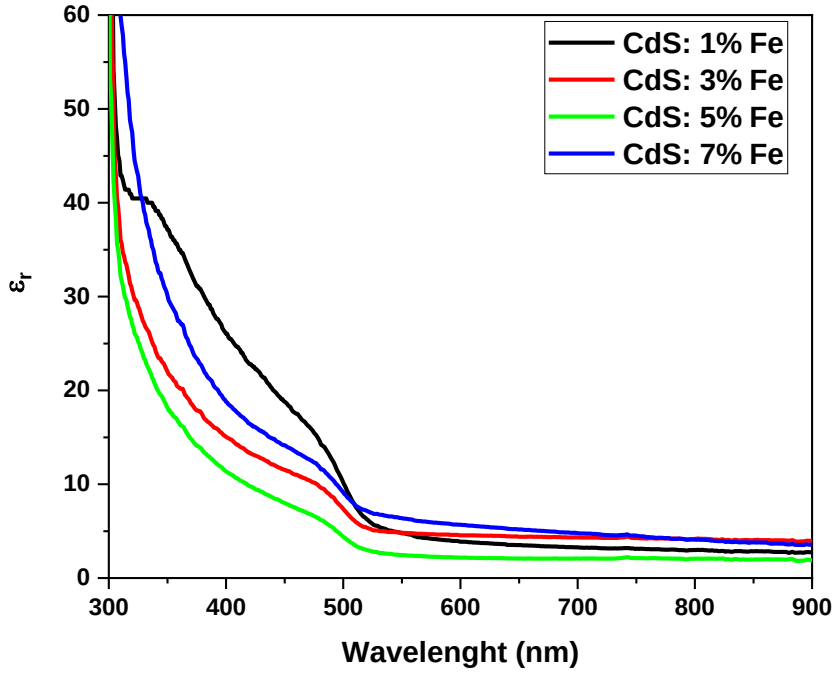

Figure 14. Real part of the dielectric constant of iron-doped CdS films.

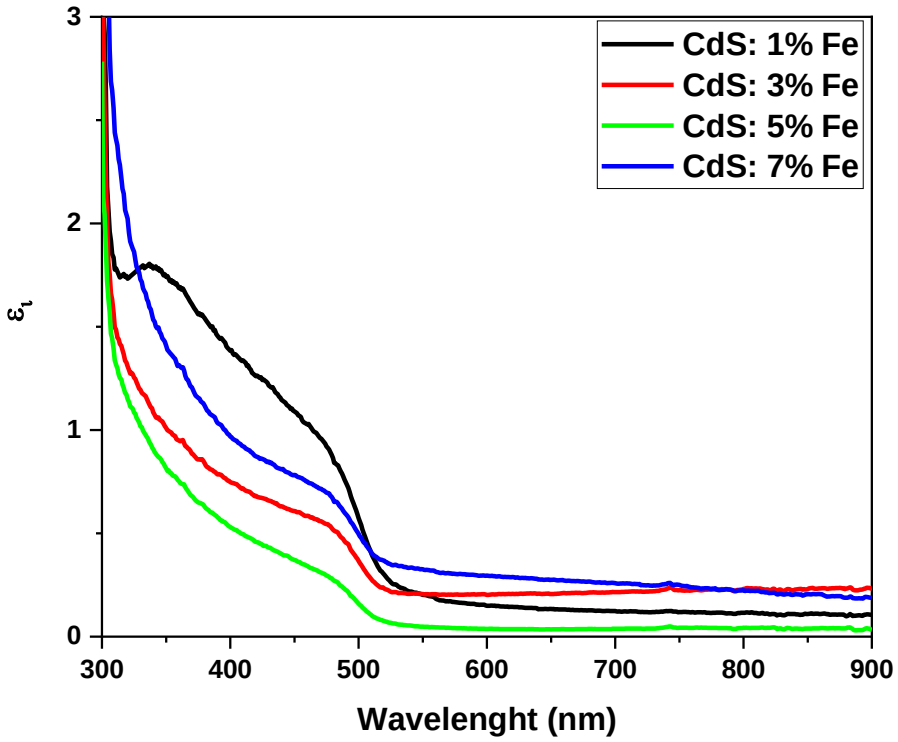

Figure 15. The imaginary part of the dielectric constant of Fe-doped CdS films.

The optical conductivity of spin-coated Fe-doped CdS thin films has been calculated from the following equation:

$$\sigma_{op} = \frac{\alpha nc}{4\pi} \quad (11)$$

Figure 16 depicts the evolution of the optical conductivity of Fe-doped CdS layers deposited by the spin coating technic. The figure shows a decrease in the optical conductivity by increasing Fe content from 1 wt% to 5 wt%, which indicates a reduction in the absorption edge toward a shorter wavelength. This behavior may be caused by decreased electron excitation due to increased incident photon energy [36, 37].

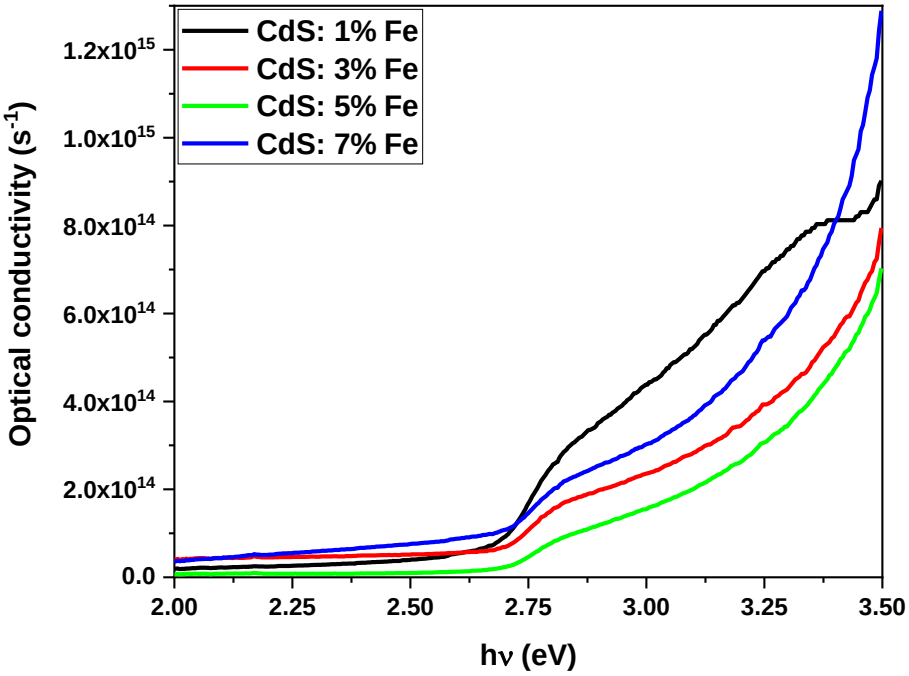

Figure 16. Optical conductivity of iron-doped CdS films.

3.5. Electrical properties.

The voltage-current characteristics at room temperature using the four-point technique and the electrical resistivity value of iron-doped Cadmium sulfide films were presented in Figure 17. We can notice a linear ohmic contact behavior in all films. The resistivity is calculated from the slope of each curve, the minimum value of the order of $4.6.10^5$ Ω.cm for the samples prepared with an atomic ratio of [Fe]/[Cd] equal 5 at.%. The substitution of Cd^{2+} ions by Fe^{3+} ions in the lattice can explain a decrease in the resistivity, which gives more charge carriers in the material. Films resistivity, however, increases at high Fe concentrations, which is caused by the formation of Fe_2O_3 in the grain boundaries, which agrees with XRD measurements. Similar results were found for nickel-doped cadmium sulfide films elaborated by the spray pyrolysis technique [29].

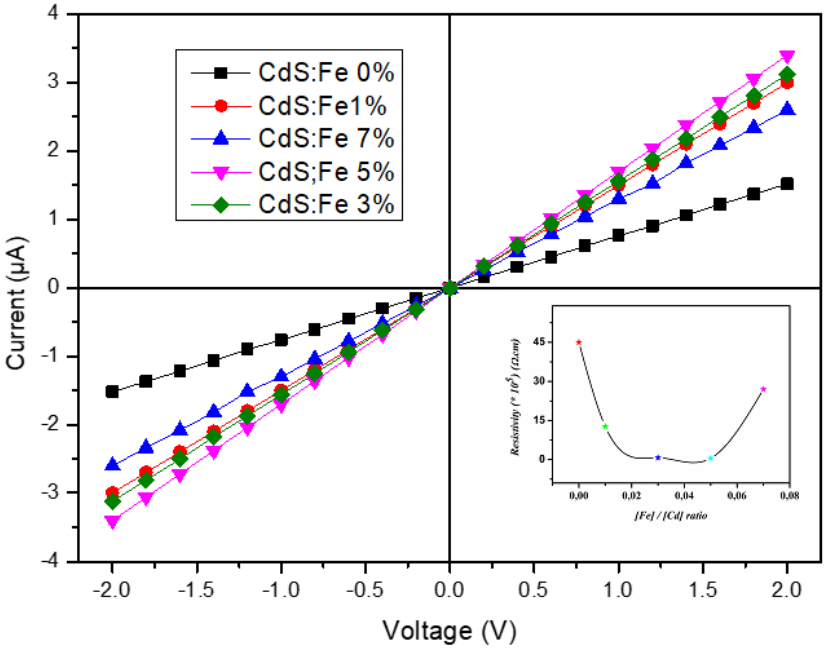

Figure 17. I-V curves and resistivity of pure and Fe-doped CdS films.

4. Conclusions

Electrical, optical and structural properties of Fe-doped CdS films elaborated by the spin-coated process have been investigated by varying the [Fe]/[Cd] molar ratios. The XRD analysis revealed a polycrystalline hexagonal (wurtzite) structure with the (002) preferential orientation for Un-doped and Fe-doped CdS samples. High Fe doping concentration leads to the appearance of the Fe_2O_3 secondary phase. Microstructural parameters such as crystallite size, strain, and stress were determined for films deposited. The morphological study shows relatively smooth surfaces composed of homogeneous and continuous nanocrystalline grains with a few quantities of voids. The spin-coated films reveal good transmittance in the visible and near-infrared regions, and the band gap increases for low Fe concentrations. The electrical measurements show that doping with an amount less than 5% Fe decreased the resistivity of CdS films. In contrast, this resistivity increases with further doping due to the probable segregation of non-conductive iron oxide at the grain boundaries.

We concluded that high transparency and low resistivity make iron-doped CdS films elaborated by spin coating a potential material adequately useful as a window and buffer layer in CdTe, CIGS, and CZTS solar cells to improve photovoltaic efficiency.

Funding

This research received no external.

Acknowledgments

This research has no acknowledgment.

Conflicts of Interest

The authors declare no conflict of interest.

Reference

1. Bai, H.; Guo, H.; Tan, Y.; Wang, J.; Dong, Y.; Liu, B.; Xie, Z.; Guo, F.; Chen, D.; Zhang, R.; Zheng, Y. Facile synthesis of mesoporous CdS/PbS/SnO_2 composites for high-selectivity H2 gas sensor. *Sens. Actuators B: Chem.* **2021**, *340*, 129924, https://doi.org/10.1016/j.snb.2021.129924.
2. Gao, T.; Li, Q.H.; Wang, T.H. CdS nanobelts as photoconductors. *Appl. Phys. Lett.* **2005**, *86*, 173105, https://doi.org/10.1063/1.1915514.
3. Reddy B, K.S.; Veeralingam, S.; Borse, P.H.; Badhulika, S. Synchronous enhancement of responsivity, response time and, spectral range in solution processed CdS photodetector upon modification with PEDOT:PSS. *J. Alloys Compd.* **2022**, *919*, 165775, https://doi.org/10.1016/j.jallcom.2022.165775.
4. Maybodi, A.S.; Malek, M.R.S. In-situ synthesis of high stable CdS quantum dots and their application for photocatalytic degradation of dyes. *Spectrochim. Acta A Mol. Biomol. Spectrosc*. **2016**, *152*, 156-164, http://dx.doi.org/10.1016/j.saa.2015.07.052.
5. Li, J.; Zhao, Z.; Li, Z.; Yang, H.; Yue, S.; Tang, Y.; Wang, Q. Construction of immobilized films photocatalysts with CdS clusters decorated by metal Cd and BiOCl for photocatalytic degradation of tetracycline antibiotics. *Chin. Chem. Lett.* **2022**, *33*, 3705-3708, https://doi.org/10.1016/j.cclet.2021.10.080.
6. Erturk, K.; Isik, S.; Aras, O.; Kaya, Y. Investigation of structural, spectral, optical and non-linear optical properties of nanocrystal CdS: Electrodeposition and quantum mechanical studies. *Optik* **2021**, *243*, 167469, https://doi.org/10.1016/j.ijleo.2021.167469.
7. Pakštas, V.; Grincienė, G.; Kamarauskas, E.; Giraitis, R.; Skapas, M.; Selskis, A.; Juškėnas, R.; Niaura, G.; Franckevičius, M. Impact of CdS layer thickness on the composition, structure and photovoltaic performance of superstrate CZTSSe solar cells. *Sol. Energy* **2020**, *207*, 1231-1239, https://doi.org/10.1016/j.solener.2020.07.052.
8. Mondal, B.K.; Mostaque, S.K.; Rashid, M.A.; Kuddus, A.; Shirai, H.; Hossain, J. Effect of CdS and In_3Se_4 BSF layers on the photovoltaic performance of PEDOT:PSS/n-Si solar cells: Simulation based on experimental data. *Superlattices Microstruct.* **2021**, *152*, 106853, https://doi.org/10.1016/j.spmi.2021.106853.
9. Lv, W.; Lei, Y.; Deng, J.; Fang, J.; Huang, W. Zn-doped CdS/CdSe as efficient strategy to enhance the photovoltaic performance of quantum dot sensitized solar cells. *Sol. Energy* **2022**, *232*, 398-408, https://doi.org/10.1016/j.solener.2022.01.006.
10. Waqar, M.; Junaid, A.; Andrew, T.; Awan, S.; Jackman, M.; Anwarul, H.; Hassan, M.U.; Nazar, A.S. Role of Ag^+ substitutional defects on the electronic and optical properties of n-type CdS thin films semiconductor for sustainable and stable window layer in solar cells technology. *Opt. Mater.* **2018**, *85*, 143-152, https://doi.org/10.1016/j.optmat.2018.08.056.
11. Bala, V.; Tripathi, S.K.; Kumar, R. Optical properties of Ga and in doped CdS nanocomposites: An experimental and first principles study. *Mater. Lett.* **2015**, *149*, 18-21, http://dx.doi.org/10.1016/j.matlet.2015.02.094.
12. Jothibas, M.; Sankar, M.; Muthuvel, A.; Srinivasan, S.; Elayaraja, M. Enhanced sunlight irradiated photocatalytic activity of Sn doped CdS nanoparticles for the degradation of organic pollutants. *Inorg. Chem. Commun.* **2022** , *136*, 109149, https://doi.org/10.1016/j.inoche.2021.109149.
13. Yılmaz, S.; Atasoy, Y.; Tomakin, M.; Bacaksız, E. Comparative studies of CdS, CdS:Al, CdS:Na and CdS:(Al–Na) thin films prepared by spray pyrolysis. *Superlattices Microstruct*. **2015**, *88*, 299-307, https://doi.org/10.1016/j.spmi.2015.09.021.

14. Mukherjee, A.; Ghosh, P.; Aboud, A.A.; Mitra, P. Influence of copper incorporation in CdS: Structural and morphological studies. *Mater. Chem. Phys.* **2016**, *184*, 101-109, https://doi.org/10.1016/j.matchemphys.2016.09.030.
15. Nazir, A.; Toma, A.; Shah, N. A.; Panaro, S.; Butt, S.; Sagar, R.R.; Raja, W.; Rasool, K.; Maqsood, A. Effect of Ag doping on opto-electrical properties of CdS thin films for solar cell applications. *J. Alloys Compd.* **2014**, *609*, 40-45, http://dx.doi.org/10.1016/j.jallcom.2014.04.144.
16. Ashith, V.K.; Priya, K.; Rao, G.K. The electrical properties of n-CdS/p-CdTe and n-ZnS/p-CdTe heterojunctions fabricated by a combination of SILAR and vacuum deposition techniques. *Physica B: Condensed Matter* **2021**,*614*, 413025, https://doi.org/10.1016/j.physb.2021.413025.
17. Erturk, K.; Isik, S.; Aras, O.; Kaya, Y. Investigation of structural, spectral, optical and non-linear optical properties of nanocrystal CdS: Electrodeposition and quantum mechanical studies. *Optik* **2021**, *243*, 167469, https://doi.org/10.1016/j.ijleo.2021.167469.
18. Rondiya, S.; Rokade, A.; Funde, A.; Kartha, M.; Pathan, H.; Jadkar, S. Synthesis of CdS thin films at room temperature by RF-magnetron sputtering and study of its structural, electrical, optical and morphology properties. *Thin Solid Films* **2017**, *631*, 41-49, https://doi.org/10.1016/j.tsf.2017.04.006.
19. Rascón, J.I.C.; Reyes, J.D.; Pacheco, A.F.; Morales, R.L.; Álvarez-Ramos, M.E.; Balderas-López, J.A. Structural and optical modifications of CdS properties in CdS-Au thin films prepared by CBD. *Results Phys.* **2021**, *22*, 103914, https://doi.org/10.1016/j.rinp.2021.103914.
20. Kathalingam, A.; Valanarasu, S.; Ahamad, T.; Alshehri, S.M.; Kim, H.S. Spray pressure variation effect on the properties of CdS thin films for photodetector applications. *Ceram. Int.* **2021**, *47*, 7608-7616, https://doi.org/10.1016/j.ceramint.2020.11.100.
21. Rahman, M.F.; Moon, M.A.; Ali, M.H.; Ahmmed, S.; Tabassum, S.; Hossain, J.; Ismail, A.M. A systematic study of how annealing conditions lead to the application-based microstructural, crystallographic, morphological, and optical features of spin-coated CdS thin-films. *Opt. Mater.* **2021**, *117*, 111136, https://doi.org/10.1016/j.optmat.2021.111136.
22. Gunasekaran, M.; Seenuvasakumaran, P. Structural and optical properties of CdS & Pb doped CdS thin films coated by spin coating technique. *Mater. Today: Proc.* **2022**, *49*, 2707-2711, https://doi.org/10.1016/j.matpr.2021.09.063.

Di Luccio, T.; Piscopiello, E.; Laera, A.M.; Antisar, M.V. Structural studies of thin films of semiconducting nanoparticles in polymer matrices. *Mater. Sci. Eng: C.* **2007**, *27*, 1372-1376, https://doi.org/10.1016/j.msec.2006.07.018.

23. Chtouki, T.; El Kouari, Y.; Kulyk, B.; Louardi, A.; Rmili, A.; Erguig, H.; Elidrissi, B.; Soumahoro, L.; Sahraoui, B. Spin-coated nickel doped cadmium sulfide thin films for third harmonic generation applications. *J. Alloys Compd.* **2017**, *696*, 1292-1297, https://doi.org/10.1016/j.jallcom.2016.12.089.
24. Benkhettou, N.; Rached, D.; Soudini, B.; Driz, M. High-pressure stability and structural properties of CdS and CdSe. *Phys. Status Solidi* **2004**, *241*, 101-107, https://doi.org/10.1002/pssb.200301907.
25. Bacaksiz, E.; Tomakin, M.; Altulbas, M.; Parlak, M.; Colagoklu, T. Structural, optical and magnetic properties of $Cd_{1-x}Co_xS$ thin films prepared by spray pyrolysis. *Physica B: Condens. Mat.* **2008**, *403*, 3740-3745, https://doi.org/10.1016/j.physb.2008.07.006.
26. Kadam, L.D.; Patil, P.S. Thickness-dependent properties of sprayed cobalt oxide thin films. *Mater. Chem. Phys.* **2001**, *68*, 225-232, https://doi.org/10.1016/S0254-0584(00)00367-9.
27. Herrera-Molina, D.; Diosa, J.E.; Fernandez-Perez, A.; Mosquera-Vargas, E. Influence of aluminum doping on structural, morphological, vibrational, and optical properties of CdS thin films obtained by chemical bath deposition. *Mater. Sci. Eng.: B* **2021,** *273*, 115451, https://doi.org/10.1016/j.mseb.2021.115451.
28. Rmili, A.; Ouachtari, F.; Bouaoud, A.; Louardi, A.; Chtouki, T.; Elidrissi, B.; Erguig, H. Structural, optical and electrical properties of Ni-doped CdS thin films prepared by spray pyrolysis. *J. Alloys Compd.* **2013**, *557*, 53-59, https://doi.org/10.1016/j.jallcom.2012.12.136.
29. Veerathangam, K.; Pandian, M.S.; Ramasamy, P. Incorporation of Co^{2+} in CdS quantum dots for solar cell applications. *Mater. Sci. Semicond. Process.* **2020**, *108*, 104869, https://doi.org/10.1016/j.mssp.2019.104869.
30. Fujita, S.; Tanaka, H.; Fujita, S. MBE growth of wide band gap wurtzite MgZnO quasi-alloys with MgO/ZnO superlattices for deep ultraviolet optical functions. *J. Cryst. Growth.* **2005**, *278*, 264-267, https://doi.org/10.1016/j.jcrysgro.2005.01.029.
31. Deshmukh, S.K.; Kokate, A.V.; Sathe, D.J. Studies on electrodeposited $Cd_{1-x}Fe_xS$ thin films. *Mater. Sci. Eng.: B.* **2005**, *122*, 206-210, https://doi.org/10.1016/j.mseb.2005.06.001.

32. Garmim, T.; Bouabdalli, E.; Soussi, L.; El Jouad, Z.; Mghaiouini, R.; Louardi, A.; Hartiti, B.; El Jouad, M.; Monkade, M. Opto-electrical properties of Ni and Mg co-doped CdS thin films prepared by spin coating technique. *Phys. Scr.* **2021**, *96*, 045813, https://doi.org/10.1088/1402-4896/abe3c0.
33. AlFaify, S.; Haritha, L.; Manthrammel, M.A.; Ganesh, V.; Chandekar, K.V.; Shaikh, S.S.; Shkir, M. Fabrication and characterization of Sn:CdS films for optical-nonlinear-limiting applications. *Optic Laser. Technol.* **2020**, *126*, 106122, https://doi.org/10.1016/j.optlastec.2020.106122.
34. Garmim, T.; Chahib, S.; Soussi, L.; Mghaiouini, R.; El Jouad, Z.; Louardi, A.; Karzazi, O.; El Jouad, M.; Hlil, E.K.; Hartiti, B.; Monkade, M. Optical, electrical and electronic properties of SnS thin films deposited by sol gel spin coating technique for photovoltaic applications. *J Mater Sci: Mater Electron.* **2020**, *31*, 20730-20741, https://doi.org/10.1007/s10854-020-04586-y.
35. El Radaf, I.M.; Hamid, T.A.; Yahia, I.S. Synthesis and characterization of F-doped CdS thin films by spray pyrolysis for photovoltaic applications. *Mater. Res. Express.* **2018**, *5*, 066416, https://doi.org/10.1088/2053-1591/aaca7b.
36. Shkir, M.; Chandekar, K.V.; Khan, A.; El-Toni, A.M.; Ashraf, I.M.; Benghanem, M.; Adil, S.F.; Ansari, A.A.; Ghaithan, H.; AlFaify, S. Structural, morphological, vibrational, optical, and non-linear characteristics of spray pyrolyzed CdS thin films: Effect of Gd doping content. *Mater. Chem. Phys.* **2020**, *255*, 123615, https://doi.org/10.1016/j.matchemphys.2020.123615.